metals

MDPI

Article

Superelasticity of Geometrically Graded NiTi Shape Memory Alloys

Weimei Chen, Rui Xi, Hao Jiang, Xiaoqiang Li, Guiwei Dong * and Xiebin Wang

Key Laboratory for Liquid-Solid Structural Evolution and Processing of Materials (Ministry of Education), Shandong University, Jingshi Road 17923, Jinan 250061, China; weimei.chen2022@hotmail.com (W.C.); rui.xi2020@hotmail.com (R.X.); hao.jiang2020@hotmail.com (H.J.); lixiaoqiang3314@163.com (X.L.); xiebin.wang@email.sdu.edu.cn (X.W.)

* Correspondence: gwdong@sdu.edu.cn; Tel.: +86-189-5419-6961

Abstract: A stress plateau with a strain of 5–8% normally occurs during the stress-induced martensite transformation (SIM) of NiTi shape memory alloys. Within the stress plateau, the correlation between the stress and strain is lost, which limits their application in certain fields which require accurate control of inelastic deformation. In order to address this limitation, a series of step-like NiTi samples with graded cross-sectional area were designed and fabricated. Multiple stress plateaus were achieved by varying the sample width and adjusting the number of steps; for instance, two and three stress plateaus were obtained in the samples with two and three steps, respectively. Also, linear force–strain response was obtained by changing gradually the width of the samples. The functional stability of the geometrically graded samples was significantly improved by incomplete recrystallization annealing (600 °C) followed by low-temperature (250 °C) aging treatment. The incompletely recrystallized specimens contained many dislocations and grain and sub-grain boundaries, which promoted the uniform precipitation of Ni_4Ti_3 nanoparticles during aging treatment. The homogeneously and densely dispersed Ni_4Ti_3 nanoparticles were able to strengthen the matrix considerably and prevent plastic activities during stress-induced martensite transformation. As a result, the functional stability of the geometrically graded NiTi samples was much improved. After aging at 250 °C for 120 h, all the samples showed a small residual strain of <1.0% after 20 loading–unloading cycles.

Keywords: shape memory alloys; NiTi; functionally graded material; superelasticity; functional stability

Citation: Chen, W.; Xi, R.; Jiang, H.; Li, X.; Dong, G.; Wang, X. Superelasticity of Geometrically Graded NiTi Shape Memory Alloys. *Metals* **2023**, *13*, 1518. https://doi.org/10.3390/met13091518

Academic Editor: Alexander V. Shelyakov

Received: 24 July 2023
Revised: 20 August 2023
Accepted: 24 August 2023
Published: 26 August 2023

1. Introduction

NiTi shape memory alloys (SMAs) show unique superelasticity (SE) and shape memory effect (SME), which originate from the reversible thermoelastic martensitic transformation between a B2-structured austenite (A) phase and a B19′-structured martensite (M) phase [1–4]. These unique properties have attracted widespread interest, including for aerospace [5–7], biomedicine [8–10], and micro-electromechanical systems [11,12]. During the stress-induced martensite transformation (SIM), a stress plateau occurs over a large strain of 5–7% [13,14]. Within the stress-plateau, the correlation between the stress and strain is lost, which limits their application in certain fields that require accurate control of inelastic deformation, such as guide wires, micro-actuators, and orthodontics [15–17].

To address this limitation, many studies have shown that microstructurally [18,19], compositionally [20,21], or geometrically [22,23] graded NiTi alloys could be designed to achieve flexible control of the mechanical performance. Microstructurally graded NiTi alloys have been achieved through gradient aging [24] or annealing [25–27], which widens the transformation stress window (i.e., the stress difference between the start and the end of SIM). For example, a linear stress–strain response for SIM was achieved by introducing a gradient distribution of Ni_4Ti_3 precipitates through gradient aging in a Ni-rich NiTi

wire [24]. A gradient superelastic behavior expands the stress window for the forward transformation to ~130 MPa. Laser surface annealing [18,28] has been reported as a promising method to tune locally the microstructure (e.g., the size of recrystallized grains) of NiTi plates to make functionally graded samples, in which transformation temperature and functional properties are tuned by varying the laser energy and scan rate. By alternately varying two sets of process parameters [29] or using a repetitive scanning strategy [30] to regulate the Ni evaporation, NiTi alloys with a compositional gradient were prepared using laser powder bed fusion techniques. Similarly, local heat treatment of Ni-rich NiTi wire by laser processing resulted in more pronounced vaporization of Ni than Ti, and thus a multi-stage SIM plateau could be achieved [31]. By welding NiTi wires with different compositions into a single unit along their length, a sample with graded transformation temperatures and graded critical stress for SIM was achieved [32].

Geometrically graded NiTi alloys are featured with a gradient change in the shape perpendicular [33] or parallel to the loading axis [34]. Compared with the abovementioned microstructurally or compositionally graded alloys, the fabrication of geometrically graded NiTi alloys is quite simple, since it is more feasible to change the shape of the samples. It has been reported that the stress window for the forward transformation could be expanded to ~220 MPa in a NiTi sample with trapezoidal shape [34]. Different stress gradients have been obtained by designing different geometries, such as linear strips, concave strips, and convex strips [35]. Geometrically graded NiTi structures with parallel design configuration were also designed [36]. During uniaxial tension, two transformation plateaus were observed in geometrically graded NiTi alloys [33,37,38], i.e., a flat stress plateau and an inclined one with a positive slope. These changes in plateau are attributed to the progressive propagation of the SIM perpendicular to the loading axis. However, inhomogeneous geometries lead to uneven deformations with locally concentrated stress, which are prone to induce plastic deformation. As a result, the geometrically graded NiTi alloys are more susceptible to functional degradation than the homogeneous specimens.

Precipitation strengthening has been widely utilized to improve the performance of metallic materials [39–42]. Ni_4Ti_3 nanoprecipitates can be introduced by aging at a temperature range from 200 °C to 550 °C in Ni-rich NiTi alloys [43–45]. However, a high-temperature solution treatment is typically required prior to the aging treatment [3], which results in the coarsening of the grains. It has been reported frequently that the distribution of Ni_4Ti_3 nanoprecipitates is not homogeneous in coarse grains [41,43,46]. Kolobova et al. [47] studied the precipitation behavior from a kinetic point of view. It was found that the precipitates are much smaller at the grain or sub-grain boundaries than in the grain interior. The heterogeneous distribution of Ni_4Ti_3 nanoprecipitates may undermine the effect of precipitation hardening [48,49]. Previous studies have shown that controlling the grain size can alter the distribution of the Ni_4Ti_3 particles. Low-temperature aging treatment of the fine-grained Ni-rich NiTi alloys (e.g., 1.7 μm [42,50]) has yielded a microstructure with homogeneously distributed Ni_4Ti_3 nanoprecipitates, and thus improved functional stability [42]. For coarse-grained NiTi alloys, the uniform precipitation of Ni_4Ti_3 nanoprecipitates can be achieved by introducing dislocation networks prior to aging treatment. Several approaches have been reported to introduce the dislocations, including repetitive temperature-induced phase transformation (i.e., thermal cycles between liquid nitrogen and boiling water [51]), stress-induced phase transformation, and ultrasonic shot peening [52]. As a result, the functional stability of the coarse-grained NiTi alloys has been improved.

In this work, a series of geometrically graded samples with different stepwise shapes was designed and fabricated. The effect of sample shape on the stress–strain response was investigated. The influence of incomplete recrystallization (600 °C) and subsequent low-temperature (250 °C) aging treatment on the functional stability of geometrically graded NiTi alloys was studied. This work will provide insight into the development of high-performance functionally graded NiTi alloys.

2. Materials and Methods

A commercial cold-rolled NiTi plate (Youyan Medical Co., Ltd., Beijing, China) with a nominal composition of Ti-50.8 at.% Ni and thickness of 0.5 mm was used. The accumulated cold deformation was around 10%. Geometrically graded samples were cut from the as-received NiTi plates along the rolling direction using wire electrical discharge machining. Figure 1 shows the detailed dimensions of the samples. A homogeneous specimen with a gauge width of 3 mm and length of 20 mm was used for comparison (Figure 1a). Figure 1b shows a two-step sample with step widths of 3 mm and 4 mm and a length of 10 mm for each step. Figure 1c shows a three-step sample with step widths of 3 mm, 3.4 mm, and 4 mm and a length of 10 mm for each stage. Figure 1d shows a sample with a continuous width transition from 3 mm to 4 mm over a length of 20 mm, named the N-step sample.

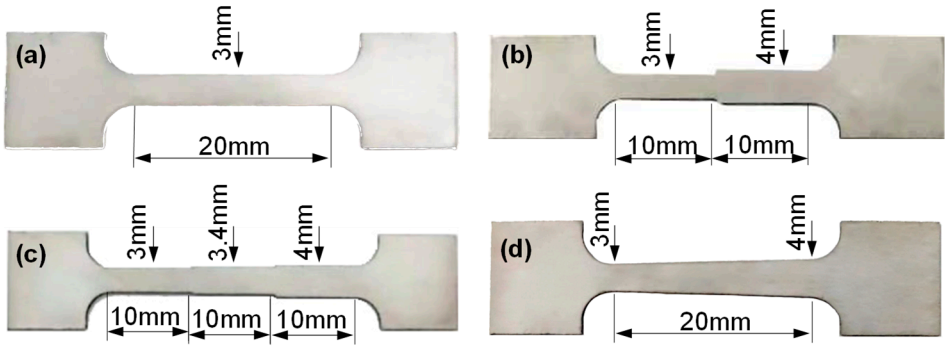

Figure 1. Dimension of the geometrically graded NiTi samples: (**a**) homogeneous sample; (**b**) two-step sample, with length of 10 mm for each step; (**c**) three-step sample, with length of 10 mm for each step; (**d**) N-step sample.

All the NiTi specimens were annealed at 600 °C for 30 min, followed by water quenching at room temperature. The characteristic transformation temperatures of the NiTi alloys, measured by differential scanning calorimetry (DSC), were −61.8 °C (M_f, martensite transformation finish temperature), −38.8 °C (M_s, martensite transformation start temperature), −22.7 °C (A_s, austenite transformation start temperature), and −6.5 °C (A_f, austenite transformation finish temperature). Low-temperature aging treatment was conducted at 250 °C for different durations from 1 h to 120 h. The microstructure of the annealed and aged samples was characterized using electron backscatter diffraction (EBSD) and transmission electron microscopy (TEM). EBSD testing was carried out using the NordlysMax3 system (Oxford Instruments, Abingdon, UK) on a JSM-7800 scanning electron microscope (JEOL, Tokyo, Japan). Samples for EBSD observation were electropolished in a solution of 21 vol% perchloric acid and 79 vol% acetic acid at room temperature. TEM characterization was performed using a Talos F200 microscope (ThermoFisher, Waltham, MA, USA), operated at 200 kV. The phase transformation behavior was studied using differential scanning calorimetry (DSC) in a DSC 3500 Sirius calorimeter (Netzsch, Selb, Germany), with a cooling/heating rate of 10 °C min^{-1}. The superelasticity was tested on a tensile test machine with a strain rate of 1.67×10^{-4} s^{-1} at room temperature.

3. Results and Discussion

3.1. Microstructure

Figure 2 shows the EBSD crystallographic orientation map and inverse pole figures of the as-annealed Ti-50.8 at.% Ni plate. Figure 2a indicates that the deformed microstructure is largely annihilated. But several deformation bands can also be observed in some areas, indicating that recovery and recrystallization occurs when annealing at 600 °C, but the short annealing duration (30 min) was insufficient for full recrystallization. The average grain size is around 27 μm, which was manually determined using the linear intercept method described by Sutou et al. [53]. Figure 2b shows the inverse pole figures with reference to the rolling direction (RD), transverse direction (TD), and normal direction (ND) of the

NiTi plate. The following relationship could be identified: RD//<110>$_{B2}$, ND//<111>$_{B2}$, indicating the presence of (111)//<110> texture in the as-annealed sample.

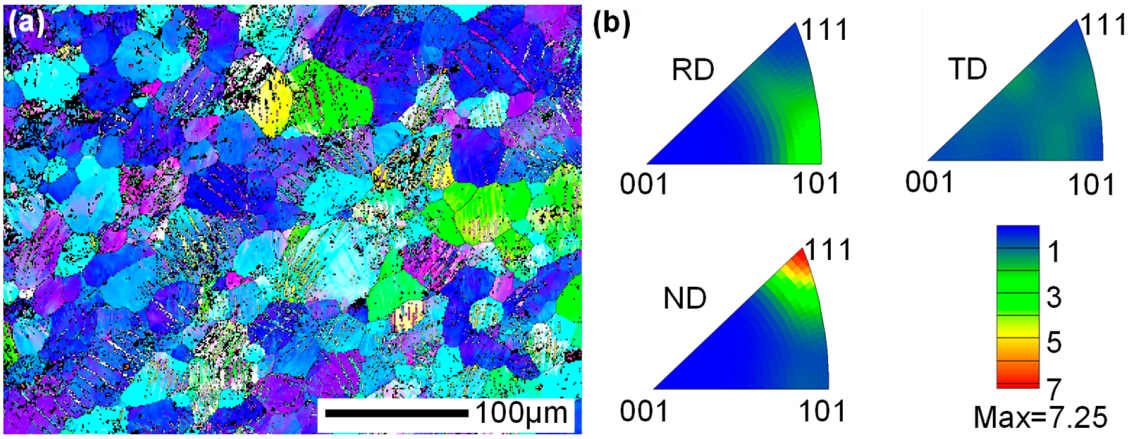

Figure 2. (**a**) EBSD orientation map of the as-annealed Ti-50.8 at.% Ni sample; (**b**) the inverse pole figures with reference to the rolling direction (RD), transverse direction (TD), and normal direction (ND), respectively.

Figure 3a–f show the TEM results of the as-annealed Ti-50.8 at.% Ni plate. Figure 3a shows that some deformed (i.e., elongated) grains still remain in the as-annealed sample. A large number of dislocations are also observed inside the elongated grains. This result is consistent with the EBSD results; the short annealing duration (30 min) was insufficient for full recrystallization. Selected area electron diffraction (SAED) pattern (Figure 3b) indicates that the as-annealed sample is in B2 austenite phase at room temperature. Some ultrafine grains with size of <500 nm, as a result of recrystallization, are also observed in Figure 3c. Figure 3d shows that a high density of dislocation also exists at the grain boundaries and in the grain interior of the equiaxial grains. Some particles with size around 1 μm are detected in Figure 3e. The corresponding SAED pattern (Figure 3f) indicates that the particles are Ti_2Ni. This indicates that the low annealing temperature (600 °C) was insufficient to dissolve the Ti-rich particles.

Figure 3g–l show the TEM images of the as-annealed sample after aging at 250 °C for 120 h. Some elongated grains are observed in Figure 3g. Figure 3h–j show the high-resolution TEM (HRTEM) image of the NiTi matrix, and the corresponding fast Fourier transforming (FFT) pattern and schematic presentation of the FFT pattern, respectively. Figure 3i,j clearly show the 1/7{321}$_{B2}$ spots (marked by green arrow) for the Ni_4Ti_3 nanoprecipitates along the [111]$_{B2}$ zone axis. This indicates that Ni_4Ti_3 particles are formed in the matrix after long-term aging treatment, consistent with previous studies [42,50]. The nucleation of Ni_4Ti_3 precipitates is energetically favorable in the places of B2 austenite lattice distortion, dislocations, grain boundaries, and sub-grain boundaries [3,54]. The diffraction spots at 1/3<110>$_{B2}$ (marked by yellow arrow) are also identified, indicating that the aged samples are in the R-phase at room temperature [55]. Some Ti_2Ni particles are also observed in the NiTi alloy (Figure 3k,l). According to EDS point analysis in Figure 3k, the Ti content of the particle is about twice the Ni content. The HRTEM image and the corresponding FFT pattern (Figure 3f) indicate the Ti_2Ni structure. The Ti_2Ni particles may have formed during the casting process.

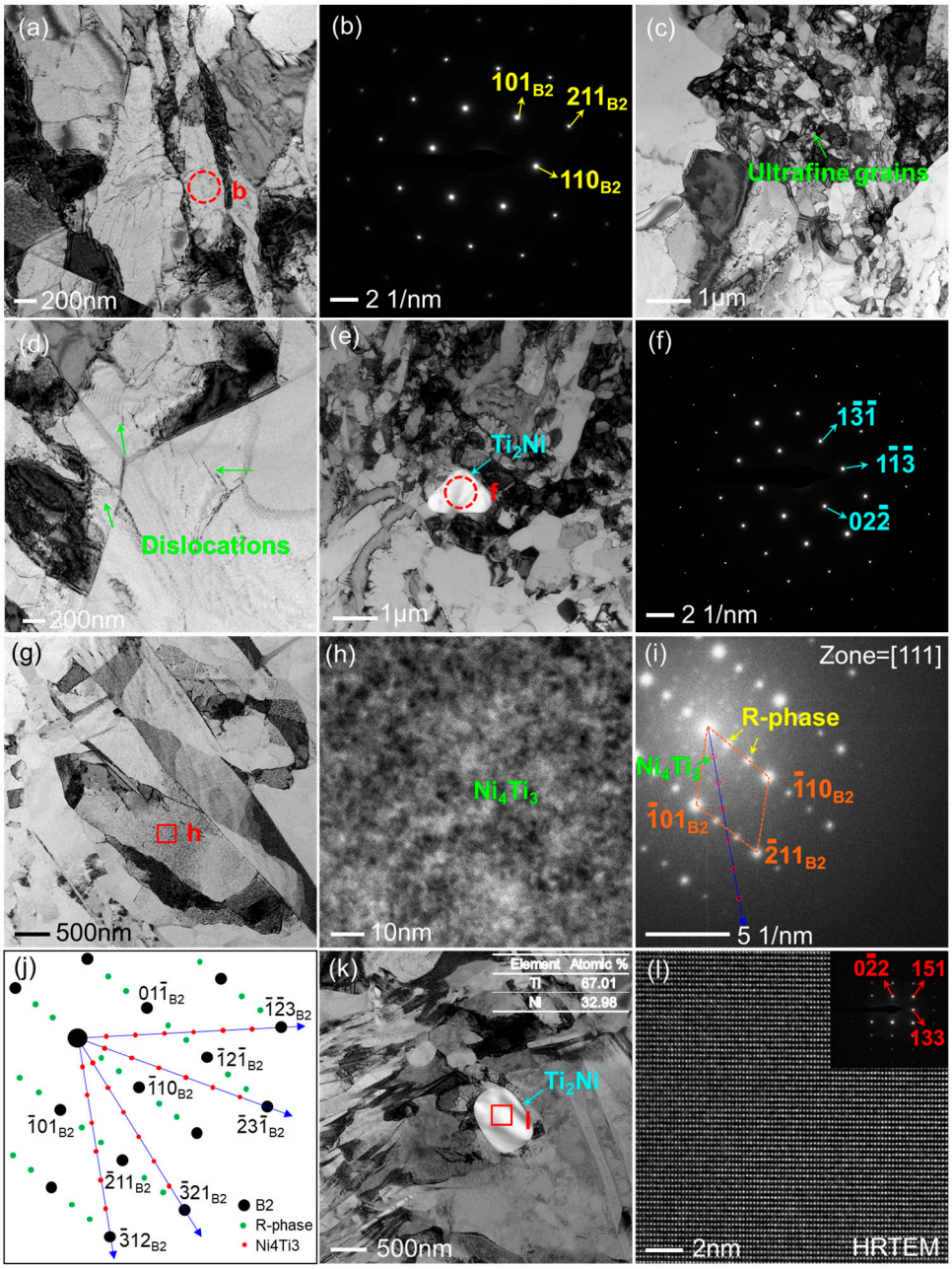

Figure 3. TEM images of the as-annealed (600 °C, 30 min) Ti-50.8 at.% Ni alloy: (**a**) TEM bright field (BF) image, (**b**) selected area electron diffraction (SAED) pattern of the red circle in (**a**), (**c**–**e**) high-magnification TEM-BF images and (**f**) SAED pattern of the red circle in (**e**). TEM images of the sample after aging at 250 °C for 120 h: (**g**) TEM-BF image, (**h**) high-resolution TEM image of the red rectangle in (**g**), (**i**) fast Fourier transforming (FFT) pattern of (**h**), (**j**) schematic presentation of FFT in (**i**), (**k**) TEM bright field (BF) image and (**l**) high-resolution TEM image and the corresponding FFT pattern of the red rectangle in (**k**).

3.2. Transformation Behavior

Figure 4a–g show the transformation behavior of the NiTi samples after aging at 250 °C for different durations from 0 h to 120 h. The martensite (M_p) and R-phase (R_p) transformation peak temperatures are summarized in Figure 4h. The transformation heat of martensite and R-phase transformation are summarized in Figure 4i. The as-annealed sample shows a one-stage A→M transformation during cooling, and M→A transformation during heating. The latent heat of the martensitic transformation is 19.3 J/g (Figure 4i),

which is less than that reported in the literature (21–29 J/g [56]). This is because the martensitic transformation is suppressed due to the incomplete recrystallization, where numerous dislocations and fine grains are present within the samples (Figure 3). Upon aging at 250 °C for short times (i.e., 1 h and 4 h), a two-stage A→R→M transformation is observed during cooling. Further increasing the aging time to 12 h-120 h, the martensite transformation peak disappears, and only A→R transformation during cooling is detected.

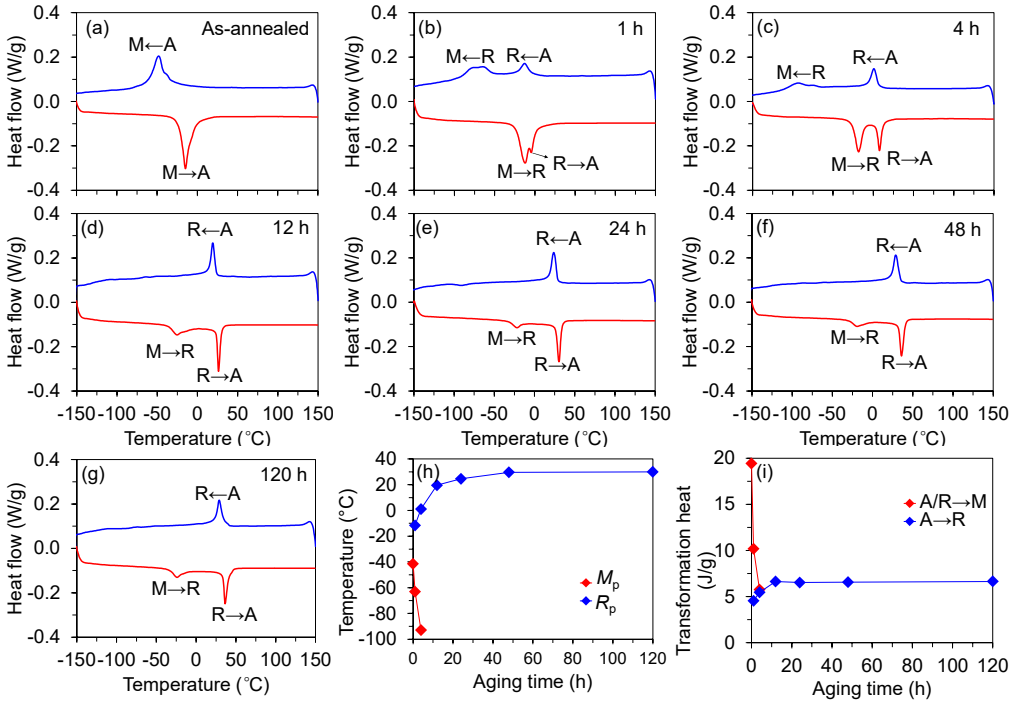

Figure 4. (**a**–**g**) DSC curves of the as-annealed NiTi samples after aging at 250 °C for different durations (from 0 h to 120 h); (**h**) variation of martensite and R-phase peak temperature with aging time; (**i**) variation of transformation heat of martensite and R-phase transformation with aging time. M_p and R_p represent the martensite and R-phase transformation peak temperatures, respectively.

According to Figure 4h, as the aging time increases from 1 h to 4 h, the M_p temperature decreases, while the R_p temperature increases. The reason behind this phenomenon is two-fold. First, a strain field is formed around the coherent Ni_4Ti_3 nanoprecipitates, which inhibits the martensitic transformation. The strength of strain field increases with the growth of Ni_4Ti_3 nanoprecipitates, leading to greater inhibition of the martensitic transformation. This leads to a reduction in martensitic transformation temperature (e.g., M_p) and the latent heat of the martensitic transformation (Figure 4i). Secondly, the strain field generated by the coherent Ni_4Ti_3 nanoprecipitates has a negligible effect on the R-phase transformation due to its small transformation strain associated with the A→R transformation (around 1%) [3]. Therefore, the R-phase transformation temperature is mainly related to the Ni content in the matrix. The formation of Ni_4Ti_3 nanoparticles causes the depletion of Ni in the matrix, leading to an increase in the R-phase transformation temperature. The latent heat of the R-phase transformation also increases (Figure 4i). After aging for 12 h, only the A→R peak temperature is detected during cooling due to the further suppression of the martensitic transformation. The R→M transformation takes place continuously over a wide temperature range, resulting in a non-detectable transformation peak temperature. However, an evident M→R peak temperature is observed during heating.

It has been frequently reported that multi-stage martensitic transformation with two-stage R-phase occurs in the coarse-grained (e.g., average grain size > 20 μm) Ni-rich NiTi alloys after low-temperature aging treatment [48]. The multi-stage transformation

is mainly due to the inhomogeneous distribution of Ni_4Ti_3 precipitates between the vicinity of grain boundaries and the grain interior. However, in this work, the multi-stage transformation is absent, indicating a homogeneous distribution of the Ni_4Ti_3 nanoprecipitates. This is mainly due to the presence of dislocations and ultra-fine grains, which helps the precipitation of the Ni_4Ti_3 particles in the grain interior. As a result, the homogeneous aging microstructure could be achieved.

3.3. Superelasticity

Figure 5 shows the tensile loading–unloading curves of the homogeneous and geometrically graded NiTi samples (with a tensile strain of 10%). Figure 5a shows the deformation behavior of the homogenous sample. During loading, elastic deformation of the austenite phase (stage I) occurs first, followed by the stress-induced martensite (SIM) transformation (stage II), which produces a stress (or force) plateau. Once the SIM is complete, the sample undergoes the elastic deformation of the martensite (stage III). Upon unloading, elastic strain is recovered and the stress-induced martensite reverse transformation occurs, producing a plateau with lower force level. A small residual strain is generated, caused by the plastic activities during A↔M transformation.

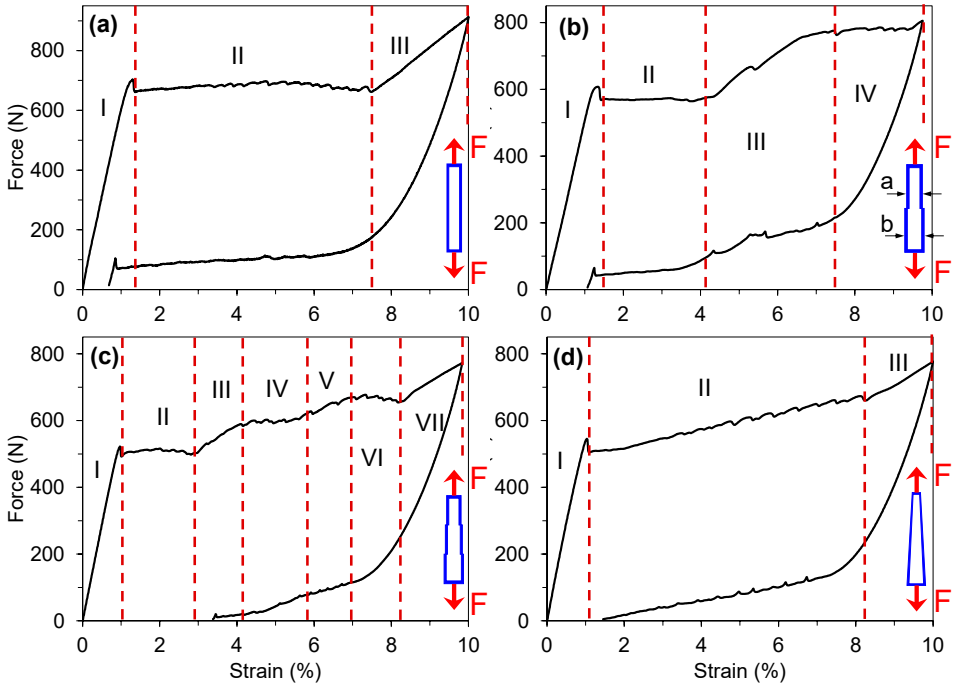

Figure 5. Tensile loading–unloading curves of the geometrically graded NiTi samples: (**a**) homogeneous sample; (**b**) two-step sample; (**c**) three-step sample; (**d**) N-step sample.

Figure 5b shows the mechanical behavior of the two-step sample (10 mm for each step), where sections a and b represent the regions with widths of 3 mm and 4 mm, respectively. Upon loading, SIM starts at the narrow region giving rise to the first force plateau (stage II). After the completion of the SIM in stage II, section a undergoes the elastic deformation of stress-induced martensite (stage III), in which the force increases with the increase in strain. When the force reaches a critical value, the SIM in the wide region is triggered, resulting in a second force plateau (section IV). Therefore, two force plateaus are obtained by changing the width of the samples.

Figure 5c shows the mechanical behavior of the three-step NiTi sample (widths of 3, 3.4, and 4 mm). Similar to the two-step specimen, SIM occurs sequentially in three different regions as the applied force increases, resulting in three plateaus, namely, sections II, IV, and VI. However, a large residual strain is observed upon unloading, since the force required to induce the SIM in section VI (i.e., widths of 4 mm) exceeds the critical value for plastic

deformation at its narrowest part (i.e., widths of 3 mm). The deformation behavior of the N-step sample is given in Figure 5d. As the loading force increases, SIM occurs successively in the trapezoidal region (stage II). The force required for the transformation gradually increases from the narrowest side (3 mm) to the widest side (4 mm), resulting in a linear force–strain relationship over a large strain (from 1% to 8%). Upon unloading, most of the strains are recovered.

Figure 6 schematically shows the sequence that triggers the SIM during loading in the homogeneous and geometrically graded NiTi samples. Figure 6a shows that the homogeneous specimen gradually undergoes SIM from austenite to martensite upon loading. The two-step specimen produces a two-step phase transformation (Figure 6b): (i) SIM occurs first in the narrow region at low loading force, and (ii) SIM occurs in the wide region at high loading force. For the N-step specimen, the cross section does not change abruptly but transitions progressively. The SIM occurs successively from the narrow side to the wide side (Figure 6c), resulting in a linear stress–strain response. This is consistent with previous studies [34,37,38].

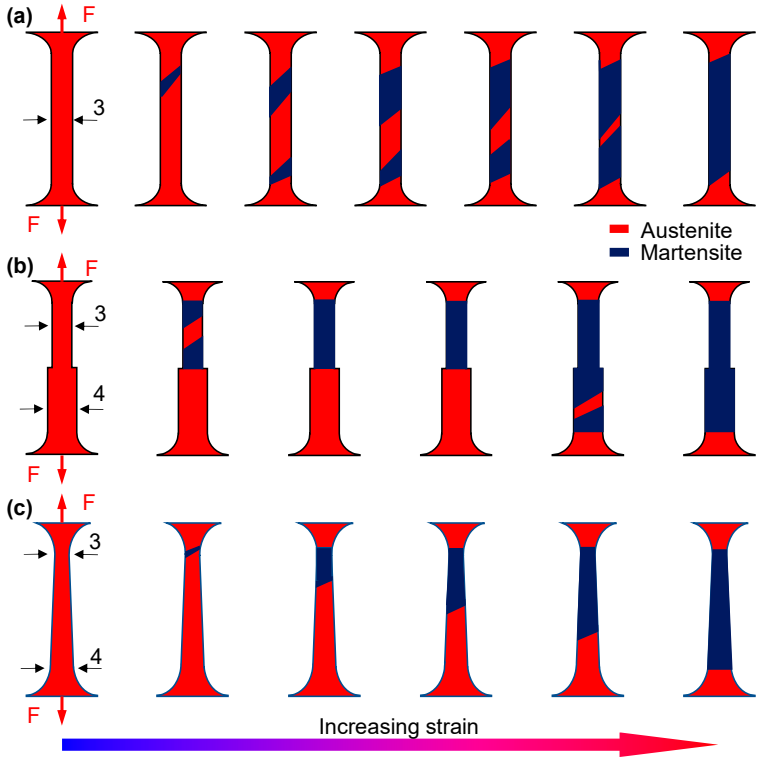

Figure 6. Schematic diagram of the phase transformation sequence of the homogeneous and geometrically graded NiTi samples during loading: (**a**) homogeneous sample; (**b**) two-step sample; (**c**) N-step sample.

As discussed above, different sample geometries result in different stress–strain responses, which offers the possibility to control the nucleation location and propagation of the SIM. This improves the controllability and flexibility of the geometrically graded NiTi samples as an actuator.

Figure 7 shows the superelastic stability of the homogeneous and geometrically graded NiTi samples after annealing. All the specimens were subjected to cyclic loading–unloading for 20 cycles with a strain of 8%. All the samples show a fast degradation of the functional stability. This is because the cyclic A↔M transformation is accompanied by plastic slip, resulting in the accumulation of residual strain. Figure 7a shows that the residual strain of homogeneous specimens is 3.4% after 20 cycles. The residual strain of the two-step sample is 4.1% (Figure 7b). The three-step sample has a residual strain of 4.2% after 20 cycles (Figure 7c). As compared with the uniform specimen, the larger residual strain of the

geometrically graded specimen is attributed to the locally concentrated deformation at the narrower region that induces more plastic deformation. However, the room temperature superelasticity of the N-step sample exhibits a residual strain of 3.5% (Figure 7d). This is mainly due to the gradual transition of the cross section that homogenizes the overall deformation and avoids the locally concentrated plastic activities. In addition, the stress–strain response (i.e., the stepwise shape of the loading–unloading curve) of geometrically graded NiTi samples disappears due to the plastic activities accompanying the cyclic A↔M transformation. For instance, the multiple force plateaus of the two-step and three-step samples disappear after 2 cycles. The results in Figure 7 indicate that geometrically graded samples are more susceptible to functional degradation than homogeneous specimens. Enhancement of the strength of the matrix is highly required to suppress plastic deformation, thus improving their functional stability.

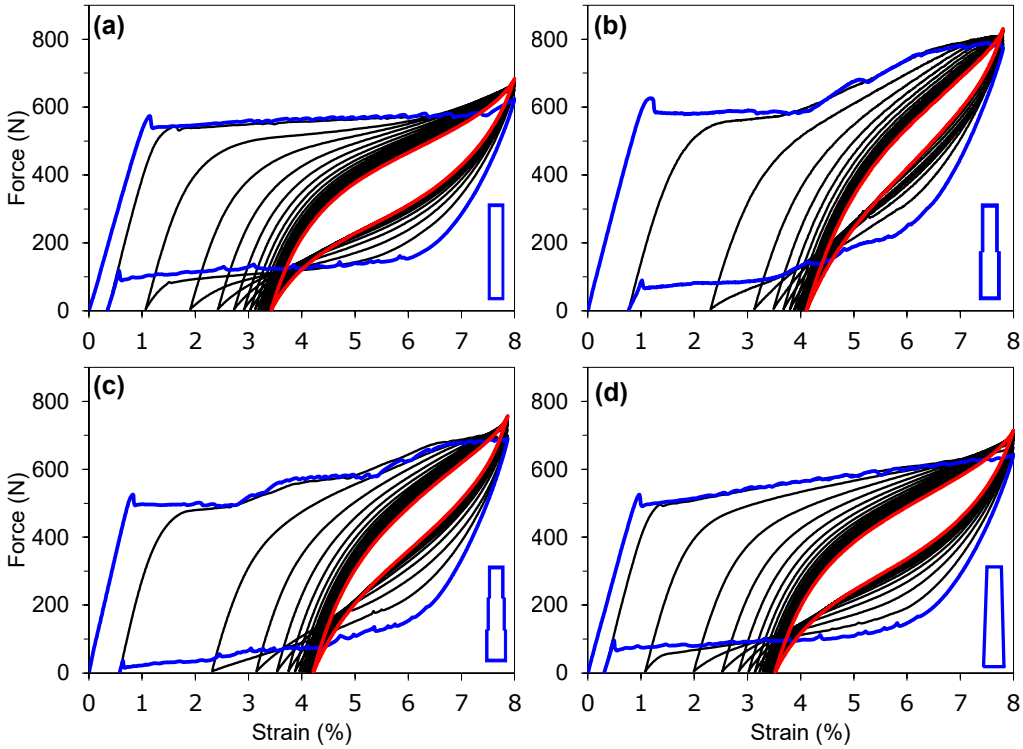

Figure 7. Superelastic curves of the as-annealed NiTi alloys with geometric gradients: (**a**) homogeneous sample; (**b**) two-step sample; (**c**) three-step sample; (**d**) N-step sample. The blue and red curves indicate the 1st and 20th cycle, respectively.

Figure 8 shows the superelastic curves of the homogeneous and geometrically graded NiTi samples after aging at 250 °C for different durations (1, 4, 12, 24, 48, and 120 h). For homogeneous samples, aging for 1 h has a negligible effect on the functional stability, and the residual strain remains 2.8% after 20 loading–unloading cycles (Figure 8a). With increasing aging time, the residual strain gradually decreases. For example, the accumulated residual strain decreases to 1.0% as the aging time increases to 120 h (Figure 8f). The improvement in superelasticity is attributed to the formation of homogeneously and densely dispersed Ni_4Ti_3 nanoprecipitates that hinders the plastic deformation during cyclic A↔M transformation.

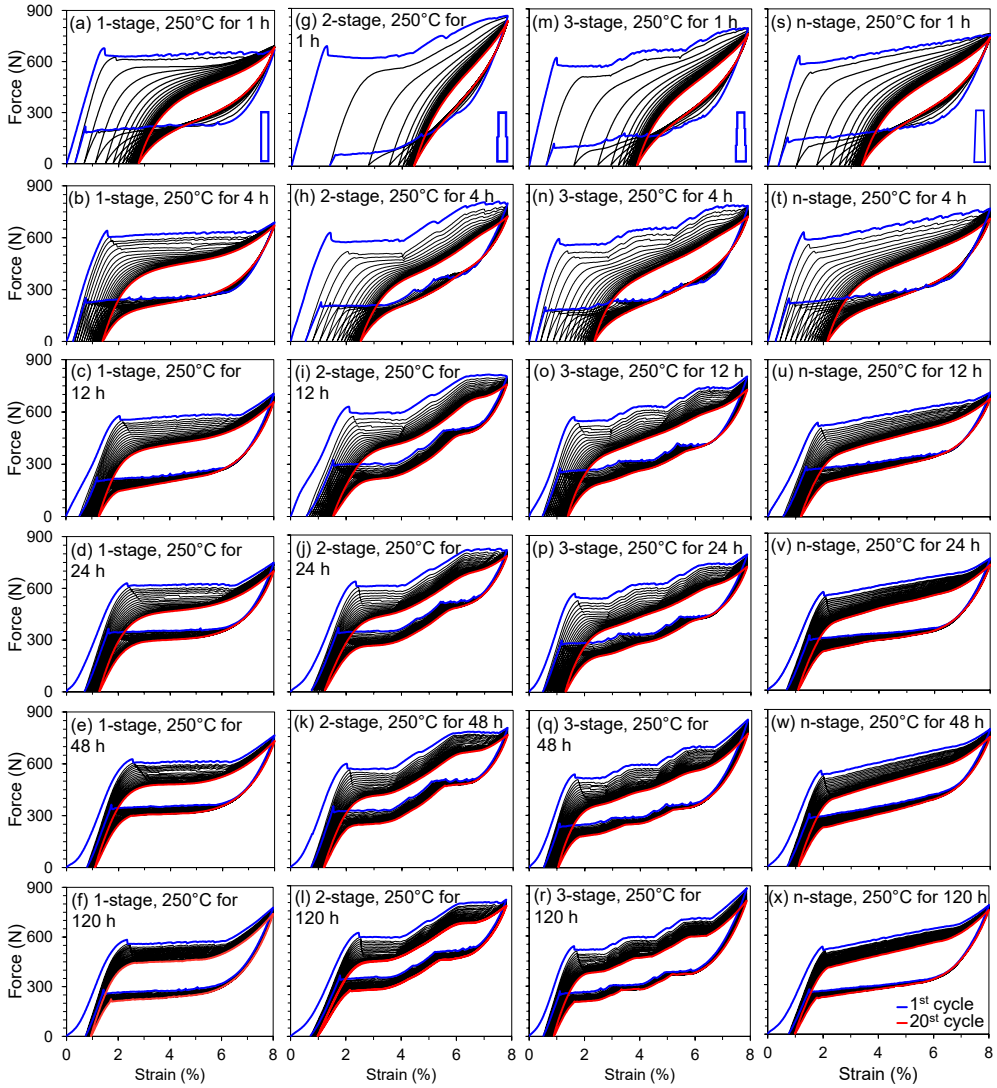

Figure 8. Superelastic curves of the homogeneous and geometrically graded NiTi samples after aging at 250 °C for different durations (1, 4, 12, 24, 48, and 120 h): (**a**–**f**) homogeneous samples; (**g**–**l**) two-step samples; (**m**–**r**) three-step samples; (**s**–**x**) N-step samples.

Similarly, the functional stability of the geometrically graded specimen is also much improved with the increase in aging time (Figure 8g–x). Although the as-annealed geometrically graded specimens are more prone to introduce plastic deformation (Figure 7), the functional stability could be improved to a level comparable to that of the homogeneous specimens after long-term aging treatment (e.g., 120 h). It is suggested that the accumulated residual strains of all the geometrically graded samples were less than 1% after 20 loading–unloading cycles after aging treatment at 250 °C for 120 h (Figure 8l,r,x).

Figure 8 also shows that the aging treatment helps to maintain the stepwise shape of the cyclic loading–unloading curves of the geometrically graded NiTi samples. For the specimens with short-term aging treatment (e.g., 1 h and 4 h), plastic deformation is generated and accumulated rapidly during cyclic A↔M transformation due to less precipitation of Ni_4Ti_3 nanoprecipitates. This results in the disappearance of the multiple force plateaus in the geometrically graded specimens after a few loading–unloading cycles. For example, the three-step specimen aged for 4 h exhibits three force plateaus in the first 5 cycles, while the plateau disappears in the subsequent 6 to 20 cycles (Figure 8n). With increasing aging time, the uniform dispersion of Ni_4Ti_3 nanoprecipitates suppresses the plastic activities, thereby increasing the number of cycles that can maintain the multiple force plateaus. After aging treatment for 120 h, the stepwise shape of the loading–unloading

curves of the two-step and three-step geometrically graded samples is still observed after 20 loading–unloading cycles (Figure 8l,r). The above results indicate that long-time aging treatment not only improves functional stability but also helps to maintain the stepwise stress–strain response of geometrically graded samples.

Figure 9 summarizes the total residual strain of the different geometrically graded samples. For the as-annealed and the short-term aged (i.e., 1 h and 4 h) specimens, a large residual strain is generated in the first few cycles due to the rapid accumulation of plastic deformation. In subsequent cycles, the residual strain increment is gradually reduced. However, the overall residual strain increment of long-term-aging-treated (i.e., 120 h) specimens is small, which is attributed to the inhibition of plastic activities by the uniform precipitation of Ni_4Ti_3 nanoparticles.

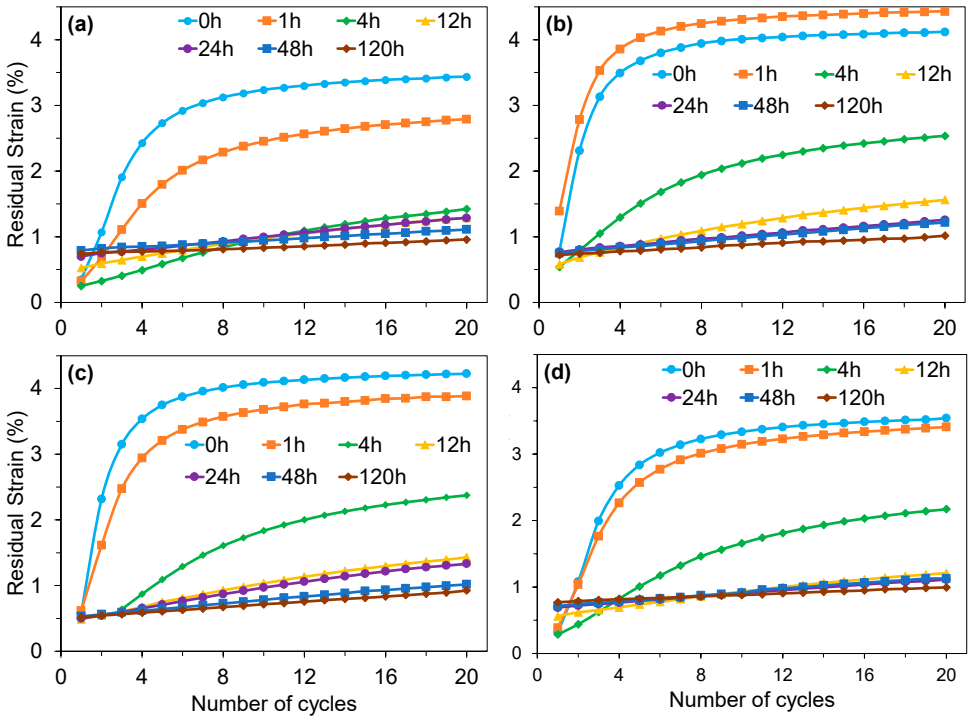

Figure 9. Effect of cycling number on the residual strain: (**a**) homogeneous samples; (**b**) two-step samples; (**c**) three-step samples; (**d**) N-step samples.

4. Conclusions

In this study, a series of geometrically graded NiTi samples were designed and fabricated. Multiple force plateaus were achieved by varying the geometries of each step. The superelastic stability of geometrically graded samples was improved through a combination of incomplete recrystallization treatment and long-term low-temperature aging treatment. The main conclusions can be drawn as follows:

(1) Altering the width and the number of steps of the geometrically graded samples can adjust their stress–strain response, resulting in multiple force plateaus over a large strain of 8%.

(2) Geometrically graded samples are more susceptible to functional degradation than homogeneous specimens due to the locally concentrated deformation at the narrower region that induces more plastic deformation.

(3) Incomplete recrystallization treatment at 600 °C for 30 min leads to a high density of dislocations and grain and sub-grain boundaries in the specimen, which are energetically favorable for the nucleation of Ni_4Ti_3 precipitates during the subsequent low-temperature aging process. This significantly improves the functional stability of the geometrically graded samples. All the geometrically graded samples aged at

250 °C for 120 h show good superelasticity, with a total residual strain of <1.0% after 20 loading–unloading cycles.

(4) The stepwise shape of the stress–strain curve (i.e., stress–strain response) of the geometric gradient samples can be maintained after long-term low-temperature aging treatment (i.e., 120 h) due to the suppression of plastic activities.

Author Contributions: Conceptualization, X.L., G.D. and X.W.; methodology, R.X., X.L. and X.W.; validation, W.C., R.X., X.L. and H.J.; formal analysis, W.C., R.X., X.L. and X.W.; investigation, W.C., R.X. and X.L.; writing—original draft preparation, W.C., R.X., H.J., G.D. and X.W.; writing—review and editing, G.D. and X.W.; visualization, W.C., R.X., H.J. and X.L.; supervision, G.D. and X.W.; project administration, G.D. and X.W.; funding acquisition, G.D. and X.W. All authors have read and agreed to the published version of the manuscript.

Funding: This work was supported by the Natural Science Foundation of Shandong Province (No. ZR2020YQ39, ZR2020ME148, and ZR2020ZD05), Taishan Scholar Foundation of Shandong Province (tsqn202211002), and the Young Scholars Program of Shandong University (No. 2018WLJH24).

Data Availability Statement: The data that support the findings of this study are available from the corresponding author upon reasonable request.

Acknowledgments: The authors acknowledge the discussions with, and assistance from, Ze Pu (Tsinghua University).

Conflicts of Interest: The authors declare no conflict of interest.

References

1. Miyazaki, S.; Otsuka, K. Deformation and transition behavior associated with the R-phase in Ti-Ni alloys. *Metall. Trans. A* **1986**, *17*, 53–63. [CrossRef]
2. Van Humbeeck, J. Shape Memory Alloys: A Material and a Technology. *Adv. Eng. Mater.* **2001**, *3*, 837–850. [CrossRef]
3. Otsuka, K.; Ren, X. Physical metallurgy of Ti–Ni-based shape memory alloys. *Prog. Mater. Sci.* **2005**, *50*, 511–678. [CrossRef]
4. Kuranova, N.N.; Makarov, V.V.; Pushin, V.G.; Ustyugov, Y.M. Influence of Heat Treatment and Deformation on the Structure, Phase Transformation, and Mechanical Behavior of Bulk TiNi-Based Alloys. *Metals* **2022**, *12*, 2188. [CrossRef]
5. Concilio, A.; Antonucci, V.; Auricchio, F.; Lecce, L.; Sacco, E. *Shape Memory Alloy Engineering for Aerospace, Structural, and Biomedical Applications*; Elsevier: Amsterdam, The Netherlands, 2021; pp. 526–623.
6. Gupta, A.; Talha, M. Recent development in modeling and analysis of functionally graded materials and structures. *Prog. Aerosp. Sci.* **2015**, *79*, 1–14. [CrossRef]
7. Oehler, S.D.; Hartl, D.J.; Lopez, R.; Malak, R.J.; Lagoudas, D.C. Design optimization and uncertainty analysis of SMA morphing structures. *Smart Mater. Struct.* **2012**, *21*, 094016. [CrossRef]
8. Chen, W.; Gu, D.; Yang, J.; Yang, Q.; Chen, J.; Shen, X. Compressive mechanical properties and shape memory effect of NiTi gradient lattice structures fabricated by laser powder bed fusion. *Int. J. Extreme Manuf.* **2022**, *4*, 045002. [CrossRef]
9. Costa, M.M.; Miranda, A.; Bartolomeu, F.; Carvalho, O.; Matos, S.; Miranda, G.; Silva, F.S. NiTi laser textured implants with improved in vivo osseointegration: An experimental study in rats. *J. Mater. Sci. Technol.* **2022**, *114*, 120–130. [CrossRef]
10. Asgarinia, F.; Parvizi, S. Biomedical applications of NiTi alloys. In *Nickel-Titanium Smart Hybrid Materials*; Elsevier: Amsterdam, The Netherlands, 2022; pp. 297–325.
11. Gangwar, K.; Gupta, D.; Anand, P.I. Parametric Investigation on laser annealing of polyimide on improving the characteristics of NiTi SMA-based bimorph towards the development of microactuators. *Sens. Actuators A Phys.* **2023**, *360*, 114536. [CrossRef]
12. Bolocan, V.; Vâlsan, D.; Chilnicean, G.; Novac, A. Optimization of thermal deflection in NiTi-based bimorph microactuators. *Mater. Today Proc.* **2021**, *45*, 4216–4220. [CrossRef]
13. Sedmák, P.; Pilch, J.; Heller, L.; Kopeček, J.; Wright, J.; Sedlák, P.; Frost, M.; Šittner, P. Grain-resolved analysis of localized deformation in nickel-titanium wire under tensile load. *Science* **2016**, *353*, 559–562. [CrossRef]
14. Shariat, B.S.; Liu, Y.N.; Rio, G. Pseudoelastic behaviour of perforated NiTi shape memory plates under tension. *Intermetallics* **2014**, *50*, 59–64. [CrossRef]
15. Sutou, Y.; Omori, T.; Furukawa, A.; Takahashi, Y.; Kainuma, R.; Yamauchi, K.; Yamashita, S.; Ishida, K. Development of medical guide wire of Cu-Al-Mn-base superelastic alloy with functionally graded characteristics. *J. Biomed. Mater. Res. B Appl. Biomater.* **2004**, *69*, 64–69. [CrossRef] [PubMed]
16. Williams, E.A.; Shaw, G.; Elahinia, M. Control of an automotive shape memory alloy mirror actuator. *Mechatronics* **2010**, *20*, 527–534. [CrossRef]
17. Rodrigues, P.F.; Fernandes, F.M.B.; Magalhaes, R.; Camacho, E.; Lopes, A.; Paula, A.S.; Basu, R.; Schell, N. Thermo-mechanical characterization of NiTi orthodontic archwires with graded actuating forces. *J. Mech. Behav. Biomed. Mater.* **2020**, *107*, 103747. [CrossRef] [PubMed]

18. Meng, Q.L.; Liu, Y.N.; Yang, H.; Shariat, B.S.; Nam, T.-H. Functionally graded NiTi strips prepared by laser surface anneal. *Acta Mater.* **2012**, *60*, 1658–1668. [CrossRef]
19. Nematollahi, M.; Safaei, K.; Bayati, P.; Elahinia, M. Functionally graded NiTi shape memory alloy: Selective laser melting fabrication and multi-scale characterization. *Mater. Lett.* **2021**, *292*, 129648. [CrossRef]
20. Meng, Q.; Yang, H.; Liu, Y.; Nam, T.-H. Compositionally graded NiTi plate prepared by diffusion annealing. *Scr. Mater.* **2012**, *67*, 305–308. [CrossRef]
21. Meng, Q.; Wu, Z.; Bakhtiari, R.; Shariat, B.S.; Yang, H.; Liu, Y.; Nam, T.-h. A unique "fishtail-like" four-way shape memory effect of compositionally graded NiTi. *Scr. Mater.* **2017**, *127*, 84–87. [CrossRef]
22. Xu, B.; Kang, G.Z. Phase field simulation on the super-elasticity, elastocaloric and shape memory effect of geometrically graded nano-polycrystalline NiTi shape memory alloys. *Int. J. Mech. Sci.* **2021**, *201*, 106462. [CrossRef]
23. Shariat, B.S.; Yang, H.; Liu, Y. Lüders band evolution in geometrically graded NiTi plates. *J. Alloys Compd.* **2023**, *936*, 168221. [CrossRef]
24. Razali, M.F.; Mahmud, A.S. Gradient deformation behavior of NiTi alloy by ageing treatment. *J. Alloys Compd.* **2015**, *618*, 182–186. [CrossRef]
25. Mahmud, A.S.; Liu, Y.N.; Nam, T.H. Design of functionally graded NiTi by heat treatment. *Phys. Scr.* **2007**, *T129*, 222–226. [CrossRef]
26. Huang, K.; Sun, Q.P.; Yu, C.; Yin, H. Deformation behaviors of gradient nanostructured superelastic NiTi shape memory alloy. *Mater. Sci. Eng. A* **2020**, *786*, 139389. [CrossRef]
27. Chen, J.Y.; Wu, Y.P.; Yin, H. In situ multi-field investigation of grain size effects on the rate-dependent thermomechanical responses of polycrystalline superelastic NiTi. *Mater. Lett.* **2020**, *259*, 126845. [CrossRef]
28. Shariat, B.S.; Liu, Y.; Meng, Q.; Rio, G. Analytical modelling of functionally graded NiTi shape memory alloy plates under tensile loading and recovery of deformation upon heating. *Acta Mater.* **2013**, *61*, 3411–3421. [CrossRef]
29. Wang, X.B.; Speirs, M.; Kustov, S.; Vrancken, B.; Li, X.P.; Kruth, J.-P.; Van Humbeeck, J. Selective laser melting produced layer-structured NiTi shape memory alloys with high damping properties and Elinvar effect. *Scr. Mater.* **2018**, *146*, 246–250. [CrossRef]
30. Jovanova, J.; Nastevska, A.; Frecker, M. Tailoring energy absorption with functional grading of a contact-aided compliant mechanism. *Smart Mater. Struct.* **2019**, *28*, 084003. [CrossRef]
31. Michael, A.; Zhou, Y.N.; Khan, M.I. Experimental validation of a one-dimensional model for monolithic shape memory alloys with multiple pseudoelastic plateaus. *J. Intell. Mater. Syst. Struct.* **2016**, *27*, 2102–2111. [CrossRef]
32. Sevilla, P.; Martorell, F.; Libenson, C.; Planell, J.A.; Gil, F.J. Laser welding of NiTi orthodontic archwires for selective force application. *J. Mater. Sci. Mater. Med.* **2008**, *19*, 525–529. [CrossRef]
33. Bakhtiari, R.; Shariat, B.S.; Motazedian, F.; Wu, Z.G.; Zhang, J.S.; Yang, H.; Liu, Y.N. Complex transformation field created by geometrical gradient design of NiTi shape memory alloy. *Funct. Mater. Lett.* **2017**, *10*, 1740011. [CrossRef]
34. Shariat, B.S.; Liu, Y.N.; Rio, G. Hystoelastic deformation behaviour of geometrically graded NiTi shape memory alloys. *Mater. Des.* **2013**, *50*, 879–885. [CrossRef]
35. Shariat, B.S.; Meng, Q.L.; Mahmud, A.S.; Wu, Z.G.; Bakhtiari, R.; Zhang, J.S.; Motazedian, F.; Yang, H.; Rio, G.; Nam, T.-H.; et al. Functionally graded shape memory alloys: Design, fabrication and experimental evaluation. *Mater. Des.* **2017**, *124*, 225–237. [CrossRef]
36. Shariat, B.S.; Liu, Y.N.; Bakhtiari, S. Modelling and experimental investigation of geometrically graded shape memory alloys with parallel design configuration. *J. Alloys Compd.* **2019**, *791*, 711–721. [CrossRef]
37. Shariat, B.S.; Bakhtiari, S.; Yang, H.; Liu, Y.N. Controlled initiation and propagation of stress-induced martensitic transformation in functionally graded NiTi. *J. Alloys Compd.* **2021**, *851*, 156103. [CrossRef]
38. Shariat, B.S.; Bakhtiari, R.; Liu, Y.N. Nonuniform transformation behaviour of NiTi in a discrete geometrical gradient design. *J. Alloys Compd.* **2019**, *774*, 1260–1266. [CrossRef]
39. Tian, X.; Zhao, Y.; Gu, T.; Guo, Y.; Xu, F.; Hou, H. Cooperative effect of strength and ductility processed by thermomechanical treatment for Cu–Al–Ni alloy. *Mater. Sci. Eng. A* **2022**, *849*, 143485. [CrossRef]
40. Chen, Y.; Sun, S.; Zhang, T.; Zhou, X.; Li, S. Effects of post-weld heat treatment on the microstructure and mechanical properties of laser-welded NiTi/304SS joint with Ni filler. *Mater. Sci. Eng. A* **2020**, *771*, 138545. [CrossRef]
41. Wang, J.; Pan, Z.; Wang, Y.; Wang, L.; Su, L.; Cuiuri, D.; Zhao, Y.; Li, H. Evolution of crystallographic orientation, precipitation, phase transformation and mechanical properties realized by enhancing deposition current for dual-wire arc additive manufactured Ni-rich NiTi alloy. *Addit. Manuf.* **2020**, *34*, 101240. [CrossRef]
42. Wang, X.B.; Kustov, S.; Li, K.; Schryvers, D.; Verlinden, B.; Van Humbeeck, J. Effect of nanoprecipitates on the transformation behavior and functional properties of a Ti–50.8 at.% Ni alloy with micron-sized grains. *Acta Mater.* **2015**, *82*, 224–233. [CrossRef]
43. Zhou, Y.; Zhang, J.; Fan, G.; Ding, X.; Sun, J.; Ren, X.; Otsuka, K. Origin of 2-stage R-phase transformation in low-temperature aged Ni-rich Ti–Ni alloys. *Acta Mater.* **2005**, *53*, 5365–5377. [CrossRef]
44. Yi, X.Y.; Sun, K.S.; Gao, W.H.; Wang, H.Z.; Sun, B.; Yao, W.; Meng, X.L.; Gao, Z.Y.; Cai, W. The precipitation behaviors, martensite transformation and superelasticity in the aged Ni-rich Ti Ni alloy with the assist of super-high stress. *Intermetallics* **2019**, *104*, 8–15. [CrossRef]

45. Pu, Z.; Du, D.; Zhang, D.; Li, Z.; Xue, S.; Xi, R.; Wang, X.; Chang, B. Improvement of tensile superelasticity by aging treatment of NiTi shape memory alloys fabricated by electron beam wire-feed additive manufacturing. *J. Mater. Sci. Technol.* **2023**, *145*, 185–196. [CrossRef]
46. Wang, X.B.; Li, C.; Verlinden, B.; Van Humbeeck, J. Effect of grain size on aging microstructure as reflected in the transformation behavior of a low-temperature aged Ti–50.8at.% Ni alloy. *Scr. Mater.* **2013**, *69*, 545–548. [CrossRef]
47. Kolobova, A.Y.; Ryklina, E.P.; Prokoshkin, S.D.; Inaekyan, K.E.; Brailovskii, V. Study of the Evolution of the Structure and Kinetics of Martensitic Transformations in a Titanium Nickelide upon Isothermal Annealing after Hot Helical Rolling. *Phys. Met. Metall.* **2018**, *119*, 134–145. [CrossRef]
48. Wang, X.B.; Verlinden, B.; Kustov, S. Multi-stage martensitic transformation in Ni-rich NiTi shape memory alloys. *Funct. Mater. Lett.* **2017**, *10*, 1740004. [CrossRef]
49. Tong, Y.X.; Hu, K.P.; Chen, F.; Tian, B.; Li, L.; Zheng, Y.F. Multiple-stage transformation behavior of Ti 49.2 Ni 50.8 alloy with different initial microstructure processed by equal channel angular pressing. *Intermetallics* **2017**, *85*, 163–169. [CrossRef]
50. Wang, X.B.; Li, K.; Schryvers, D.; Verlinden, B.; Van Humbeeck, J. R-phase transition and related mechanical properties controlled by low-temperature aging treatment in a Ti–50.8at.% Ni thin wire. *Scr. Mater.* **2014**, *72–73*, 21–24. [CrossRef]
51. Wang, X.; Pu, Z.; Yang, Q.; Huang, S.; Wang, Z.; Kustov, S.; Van Humbeeck, J. Improved functional stability of a coarse-grained Ti-50.8 at.% Ni shape memory alloy achieved by precipitation on dislocation networks. *Scr. Mater.* **2019**, *163*, 57–61. [CrossRef]
52. Li, X.Q.; Chen, H.; Guo, W.M.; Guan, Y.J.; Wang, Z.C.; Zeng, Q.K.; Wang, X.B. Improved superelastic stability of NiTi shape memory alloys through surface nano-crystallization followed by low temperature aging treatment. *Intermetallics* **2021**, *131*, 107114. [CrossRef]
53. Sutou, Y.; Omori, T.; Yamauchi, K.; Ono, N.; Kainuma, R.; Ishida, K. Effect of grain size and texture on pseudoelasticity in Cu–Al–Mn-based shape memory wire. *Acta Mater.* **2005**, *53*, 4121–4133. [CrossRef]
54. Poletika, T.M.; Girsova, S.L.; Lotkov, A.I. Ti_3Ni_4 precipitation features in heat-treated grain/subgrain nanostructure in Ni-rich TiNi alloy. *Intermetallics* **2020**, *127*, 106966. [CrossRef]
55. Wang, X.B.; Verlinden, B.; Van Humbeeck, J. R-phase transformation in NiTi alloys. *Mater. Sci. Technol.* **2014**, *30*, 1517–1529. [CrossRef]
56. Frenzel, J.; George, E.P.; Dlouhy, A.; Somsen, C.; Wagner, M.F.X.; Eggeler, G. Influence of Ni on martensitic phase transformations in NiTi shape memory alloys. *Acta Mater.* **2010**, *58*, 3444–3458. [CrossRef]